ELSEVIER

Coordination Chemistry Reviews
206–207 (2000) 607–630

COORDINATION CHEMISTRY REVIEWS

www.elsevier.com/locate/ccr

Synthesis of nanostructured metals and metal alloys from organometallics

Kenneth E. Gonsalves [a,*], He Li [a], R. Perez [b], P. Santiago [c], M. Jose-Yacaman [c]

[a] *Department of Chemistry and Polymer Program, Institute of Materials Science, University of Connecticut, 97 North Eagleville Road, Storrs, CT 06269-3136, USA*
[b] *Laboratorio de Cernavaca, Instituto de Fisica UNAM, PO Box 139B, 62191, Cuernavaca Mor., Mexico*
[c] *Department of Materials Science, ININ, Toluca, Mexico*

Received 6 August 1999; received in revised form 3 January 2000; accepted 3 January 2000

Contents

Abstract

Techniques for the fabrication of nanostructured materials are outlined. This review covers the synthesis of nanostructured metals (Fe, Co, Ni) and metal alloys (Fe–Co, Pt–Pd, M50 steel) from corresponding organometallic precursors by various methods such as thermal

* Corresponding author. Tel.: +1-860-4866134; fax: +1-860-4864745.
E-mail address: gonsalve@vconnvm.vconn.edu (K.E. Gonsalves).

PII: S0010-8545(00)00301-5

decomposition, ultrasonic irradiation, chemical vapor deposition, laser pyrolysis, and reduction.

Keywords: Nanostructured materials; Organometallics; Nanostructured metals; Nanostructured metal alloys; Sonochemical synthesis; Chemical vapor deposition

1. Introduction

Ultrafine microstructures, having an average phase or grain size on the order of a nanometer (10^{-9} m), are classified as nanostructured materials [1]. Currently, in general terms, any material that contains grains or clusters below 100 nm, or layers, or filaments of that dimension, can be nanostructured [2]. These materials have been intensively studied in recent years, because the small size of the building blocks (particle, grain, or phase) and the high surface-to-volume ratio of these materials result in unique mechanical, optical, electronic, and magnetic properties [3]. The properties of nanostructured materials depend on the following microstructural features: (1) fine grain size and size distribution (< 100 nm); (2) the chemical composition of the constituent phases; (3) the presence of interfaces, more specifically, grain boundaries, heterophase interfaces, or the free surface; and (4) interactions between the constituent domains. The presence and interplay of these four features largely determine the properties of nanostructured materials, which are often quite different from those of the bulk materials.

Nanostructured materials bridge the gap between the molecular level and the solid state, and display unique physicochemical properties, upon which many new technological applications can be based. In nanoscale materials, a variety of size-related effects can be incorporated by controlling the sizes of the constituent components [4]. For example, nanostructured metals and ceramics have improved mechanical properties compared to conventional materials as a result of their ultrafine microstructure. In addition, nanostructured materials have the capability to be sintered at much lower temperatures than conventional powders, enabling the full densification of these materials at relatively lower temperatures. Magnetic applications of nanostructured materials include fabrication of devices with giant magnetoresistance effects, the property used by magnetic heads to read data on computer hard drives, and also the development of magnetic refrigerators that use solid magnets as refrigerants rather than compressed ozone-destroying chlorofluorocarbons [5]. In addition, nanostructured metals and ceramics seem to be good candidates for catalytic applications [6].

2. Synthesis of nanostructured materials

The synthesis of nanostructured materials from atomic or molecular sources depends on the control of a variety of 'nanoscale' attributes desired in the final

product. In general, there are broadly two synthetic techniques for nanostructured materials, namely, physical methods [7] and chemical methods [8].

The most widely used physical method involves the synthesis of single-phase metals and ceramic oxides by the inert-gas evaporation technique [9]. The generation of atom clusters by gas phase condensation proceeds by evaporating a precursor material, either a single metal or a compound at a low pressure. The evaporated atoms or molecules undergo a homogeneous condensation to form atom clusters via collisions with gas atoms or molecules in the vicinity of a cold-powder collection surface. The clusters once formed are immediately removed from the region of deposition either by natural convection of the gas or by forced gas flow to prevent further aggregation and coalescence of clusters. Sputtering is another technique used to produce nanostructured materials as well as a variety of thin films. This method involves the ejection of atoms or clusters of designated materials by subjecting them to an accelerated and highly focused beam of an inert gas such as argon or helium. Nanostructured materials can be also generated via severe mechanical deformation [10]. In this method, nanostructured materials are produced not by cluster assembly but rather by structural degradation of coarser-grained structures induced by the application of high mechanical energy. The nanometer-sized grains nucleate within the shear bands of the deformed materials converting a coarse-grained structure to an ultrafine powder. This method is very useful in generating commercial quantities of nanostructured materials.

Chemistry has also played a major role in developing new materials with novel and technologically important properties [11]. The advantage of chemical synthesis is its versatility in designing and synthesizing new materials that can be refined into the final product. The primary advantage that chemical processes offer over other methods is good chemical homogeneity, as chemical synthesis offers mixing at the molecular level. Therefore, molecular chemistry can be designed to prepare new materials by understanding the relationship between how matter is assembled at the molecular level and consequent effects on desired material macroscopic properties.

Solution chemistry is often used to prepare the precursor, which is subsequently converted to nanophase particles by nonliquid phase chemical reactions. Precipitation of a solid from a solution is a common technique for the synthesis of fine particles. The general procedure involves reactions in aqueous or nonaqueous solutions containing the soluble or suspended salts. Once the solution becomes supersaturated with the product, the precipitate is formed by either homogeneous or heterogeneous nucleation [12]. The growth of the nuclei after formation usually proceeds by diffusion, in which concentration gradients and reaction temperatures are very important in determining the growth rate of the particles. To form monodispersed particles with a very narrow size distribution, all the nuclei must form at nearly the same time, and subsequent growth must occur without further nucleation or agglomeration of the particles.

Nanostructured materials are also prepared by chemical vapor deposition (CVD) or chemical vapor condensation (CVC) [13]. In these processes, a chemical precursor is converted to the gas phase, and then undergoes decomposition at either low or atmospheric pressure to generate the nanostructured particles. These products

are then subjected to transport in a carrier gas and collected on a cold substrate, from where they are scraped and collected. The CVD method has been employed to synthesize several ceramic metals, metal alloys, and composite materials.

3. Nanostructured metals and metal alloys from organometallics

There are two main routes for the chemical synthesis of nanostructured metals and metal alloys from organometallics, i.e. thermal or ultrasonic decomposition of organometallic precursors to yield the respective elements or alloys, and reduction of organometallic precursors. We will outline various methods to prepare metals, metal alloys, and a four-component alloy of Fe, commercially known as M50 steel, from organometallics.

3.1. Synthesis of nanostructured metals from organometallics

The thermal decomposition of iron pentacarbonyl, $Fe(CO)_5$, in a high boiling solvent such as decalin is a typical example of preparing nanostructured metals from organometallics. In a variation of the above procedure, dispersions of colloidal iron are produced by the decomposition of $Fe(CO)_5$ in two kinds of polymer solutions (1) 'active' polymers such as polymers having a nitrogen nucleophile and (2) 'passive' polymers such as in polymers having an alkenyl or benzylic functionality. Examples of polymers used are: poly(butadiene), poly(styrene-co-butadiene), poly[styrene-co-4-vinylpyridine], and poly[styrene-co-*N*-vinylpyrrolidone] [14].

The role of the polymeric catalysts in particle nucleation is their action as 'dispersants', which stabilize metal particles by adsorption of a thick layer of polymer on the surface of the particles. Thus, the thermal decomposition of $Fe(CO)_5$ has been examined whereby $Fe(CO)_5$ undergoes facile valence disproportionation reactions with nitrogen nucleophiles. If analogous reactions were to occur between $Fe(CO)_5$ and nucleophilic residues [15] on a macromolecule, intermediate ligand-metal cluster compounds would be generated in the polymeric domain. It is postulated that such ligand clusters are more thermally labile than $Fe(CO)_5$ molecules in bulk solutions and, thus, are precursors to colloidal iron particles. In the absence of a polymer, the mechanism and kinetics of the decomposition of $Fe(CO)_5$ in an 'inert' hydrocarbon media such as decalin are quite complex [16]. It is not very well understood, but is certain, however, that the conversion is a sequential stepwise process in which increasingly larger clusters are formed as molecules of CO and $Fe(CO)_5$ are split out (Fig. 1). Liganded polymer–metal carbonyl compounds can also be generated in passive functional substrates, i.e. in molecules having alkenyl or benzylic (allylic) functionality [17]. The rate of decomposition of $Fe(CO)_5$ in the presence of the 'passive' polymers, poly(styrene), poly(butadiene), and poly(styrene-co-butadiene), is initially similar to that in solvent alone. However, with the formation of the intermediate polymer-bound metal carbonyl compounds, the rate of evolution of CO increases over the rate in solvent alone.

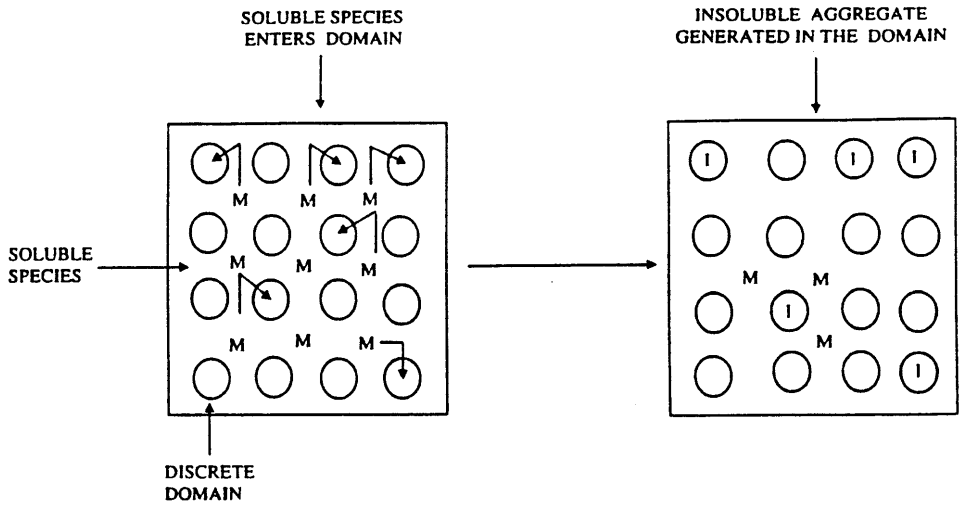

Fig. 1. Schematic illustration of Fe nanoparticles formation in an 'inert' hydrocarbon media (adapted from reference [14], pp. 1621).

Smith and Wychick have carried out the synthesis of Fe nanoparticles in the presence of butadiene-containing polymers [14]. Uniform colloidal dispersions of approximately $70 \sim 80$ Å Fe particles, which are physically very stable, were obtained. In the initial phase of the thermolysis, it was felt that the major CO-evolving reaction is that resulting in the formation of $Fe_2(CO)_9$, just as is the case in the presence of decalin alone. The 'catalyzed' reaction differs in that intermediate $[Fe(CO)_4]$ molecules can react with the isolated alkenyl residues on the polymer backbone. Subsequently, isomerization of the double bonds along the chain occurs, generating butadienyl-iron tricarbonyl residues in the polymer (Fig. 2). Particles in the dispersion that were less than 100 Å were superparamagnetic (125 emu g^{-1} of Fe at 10 000 Oe), and particles in the $100 \sim 200$ Å range had a time-dependent hysteresis.

In a slight variation of this process, Nakatani et al. [18] have developed a new metallic magnetic fluid with ε-Fe_3N fine particles dispersed in kerosene by the vapor liquid chemical reaction between iron carbonyl and NH_3. A surfactant amine (polybutenylsuccinpolyamine) was added into the reaction to produce fine colloidal dispersions. The particles showed electron diffraction patterns indexed by the ε-Fe_3N structure. The ratio of amine to $Fe(CO)_5$ had a remarkable influence on the dispersion of the iron-nitride fine particles. Varying concentrations of the surfactant yielded magnetic fluids with different agglomerations (Fig. 3). The particles in general were highly uniform in size and well dispersed without agglomeration.

In another experiment, Wonterghem et al. [19] prepared a magnetic glass, or in other terms a ferrofluid by the thermal decomposition of iron pentacarbonyl in decalin along with a surfactant (Sarkosyl-O) [20]. Usually, metallic glasses are prepared by the liquid quench or the vapor deposition techniques in which hot

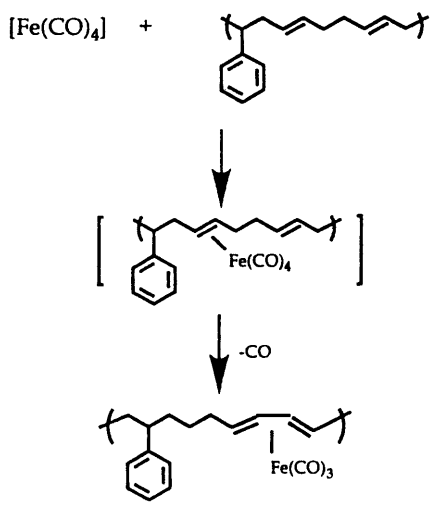

Fig. 2. Reaction of $Fe(CO)_4$ with alkenyl residues (adapted from reference [14], pp. 1621).

atoms are condensed onto a substrate kept at temperatures well below the glass transition temperature (T_g). In the case of glass formation by the carbonyl decomposition, the condensation process is presumably a vapor solid transition. The condition for glass formation is that condensed atoms are prevented from diffusing more than one atomic distance at the surface before they are fixed in position by the arrival of additional atoms. It is noteworthy that the molecules forming the metallic glass particles are at a temperature that does not exceed the boiling point of the liquid (ca. 460 K). Therefore, this carbonyl decomposition method is not based on rapid cooling from a high temperature, but, rather, the mechanism is based on growth of alloy particles in a system that is kept at a temperature below T_g. Mössbauer spectra taken at room temperature, 80, and 166 K suggest that the particles in the colloid are not pure α-Fe but an amorphous iron carbon alloy with $5 \sim 10$ at.% carbon. This type of metallic glass crystallizes into a mixture of α-Fe and iron carbides at 523 K. The Mössbauer studies [21] show that the decomposition of $Fe(CO)_5$ in the fluid results in the formation of metallic glass particles that crystallize into α-Fe and iron carbide upon heating. Fig. 4 shows the room temperature Mössbauer spectrum of the particles after heating in hydrogen at 523 K. The predominant component was unambiguously identified as the spectrum of α-Fe. The remaining weak absorption lines indicate the presence of other magnetic phases with smaller magnetic hyperfine fields. The best computer fit (Fig. 4) was obtained by including three additional six-line components of low intensity. The parameters of these components are in accordance with published values of χ-Fe_5C_2 [22]. The χ-carbide component constitutes about 8% of the spectral area corresponding to about 11 at.% carbon in the particles.

Apart from thermal decomposition methods, iron nanoparticles have also been made by ultrasonic irradiation or by laser pyrolysis of iron pentacarbonyl. A dull

powder was obtained in experiments performed by Cao et al. [23] on the sonochemical decomposition of $Fe(CO)_5$ in decane with varying solution concentrations. They obtained particles of varying sizes ($59 \sim 243$ nm) depending on the solution concentrations, with smaller particles being obtained for more dilute solutions. The nanophase iron powders do not exhibit saturation at magnetic field up to 50 kG. The magnetic moment at 50 kG varies between 42.5 emu g^{-1} for a pure $Fe(CO)_5$ solution to 12 emu g^{-1} for the most dilute solution. This result is explained on the basis that in bulk ferromagnetic materials, the local magnetic moments are organized in domains with a certain characteristic size. This yields reduction in magnetic energy of the demagnetizing field surrounding the sample. The total energy of domain boundaries grows, thoroughly as a square of the effective radius of a

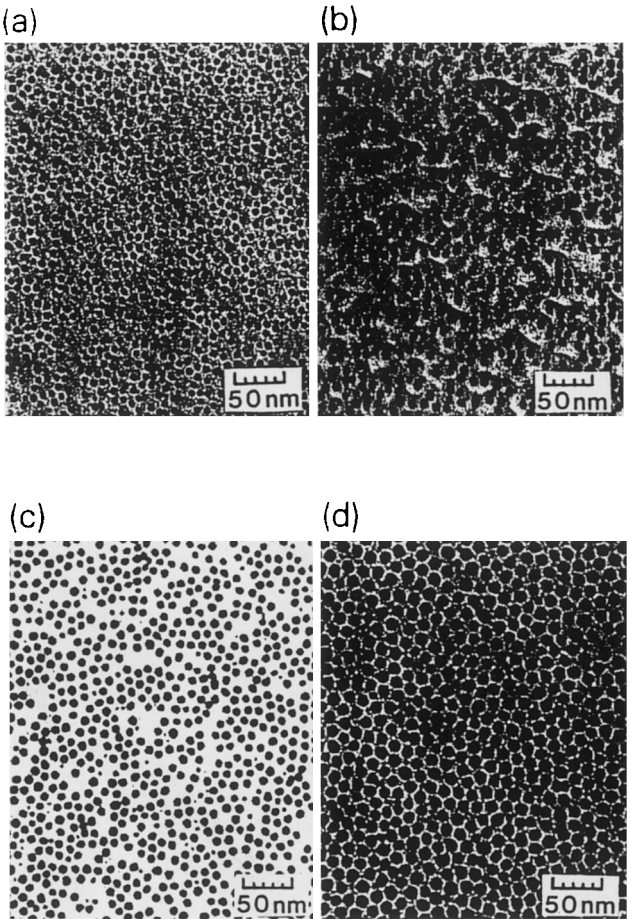

Fig. 3. Electron micrographs of iron–nitride magnetic fluids synthesized from solutions with various amounts of $Fe(CO)_5$ in 50.1 g kerosene: (a) synthesized from solution with 80 g $Fe(CO)_5$, (b) 120 g $Fe(CO)_5$, (c) 150 g $Fe(CO)_5$, and (d) 200 g $Fe(CO)_5$ (source: [18]).

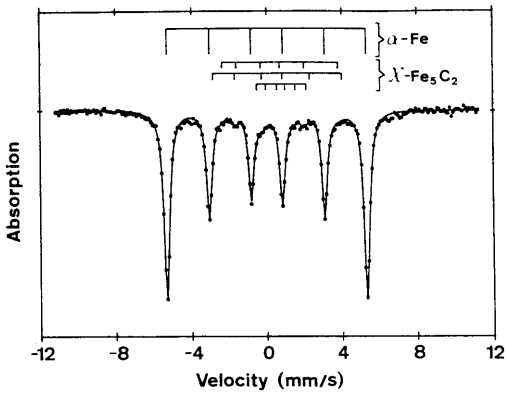

Fig. 4. Room-temperature Mössbauer spectrum of the particles after heating in hydrogen at 523 K. The full line indicates a computer fit of the spectrum with a six-line component due to α-Fe, and three six-line components due to χ-Fe_5C_2, as shown by the bar diagrams (source: [19]).

sample, whereas the magnetic energy of a demagnetizing field is proportional to third degree. At some particle size, the domain formation is not profitable anymore and particles become single-domain (all spins are oriented in a certain direction). In this case, the material becomes superparamagnetic and does not exhibit saturation. From Fig. 5 it can be seen that the pure sample is the transition state from ferromagnetism to supeparamagnetism because it still shows quite a flat region at high fields. ESR measurements on the sample showed strong signals, and it is certain that these come from the internal magnetic nature of the sample and not from the impurity contained in the amorphous iron. Interestingly, the ESR signals become stronger and sharper for more dilute solutions implying that the magnetic exchange is becoming weaker and weaker.

Suslick et al. [24] reported a sonochemical synthesis of nanostructured irons, in which a decane solution of $Fe(CO)_5$ was irradiated at 0°C with a high-intensity ultrasonic probe for 3 h under argon. The iron powder consisted of agglomerates of 20 nm particles, and these 20 nm particles consisted of smaller $4 \sim 6$ nm particles. The iron powder was amorphous, and soft ferromagnetic with a saturation magnetism of 173 emu g^{-1} and a Curie temperature in excess of 580 K. The nanostructured iron was roughly ten times more active than the 5 μm conventional iron powder in the Fischer–Tropsch process (i.e. hydrogenation of CO), in part because of the higher surface area. In a similar way, silica supported amorphous nanostructured iron was prepared by ultrasonic irradiation of decane solution of $Fe(CO)_5$ in the presence of silica gel. The iron particles were highly dispersed on a SiO_2 surface, and the particles ranged in size from 3 to 8 nm. The silica supported nanostructured iron showed an order of magnitude higher catalytic activity over conventional catalysts in the Fischer–Tropsch reaction.

In our laboratory, we have synthesized nanostructured α-Fe by sonochemical as well as thermal decomposition of $Fe(CO)_5$ in decalin [25]. In a typical reaction, for the sonochemical procedure, a dispersion of 15 g (0.076 mol) of $Fe(CO)_5$, in dry

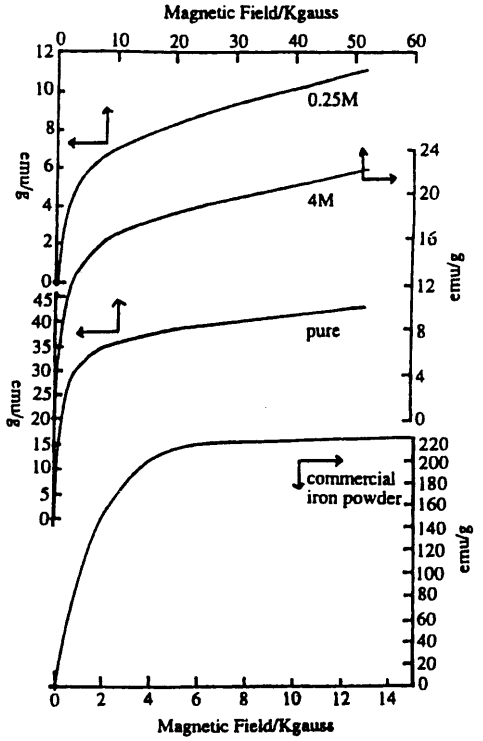

Fig. 5. Magnetization curves of commercial iron powder and amorphous iron at 100 K (source: [23]).

decalin (200 ml) was sonicated at 50% amplitude using a Sonic and Materials, VC-600 ultrasonic probe (20 kHz, 100 W cm^{-2}) for ca. 6 h at room temperature. In the thermal method, same quantities of the precursors were refluxed in decalin till the completion of the reaction. In either case, on completion of the reaction the formation of shiny metallic particles was observed on the walls of the reaction vessel. Decalin was removed by decantation and the resulting black powders were isolated and dried with heating under vacuum. These iron powders were then consolidated by vacuum hot pressing at 275 MPa at 700°C for 1 h.

The as-synthesized iron powders were amorphous by X-ray diffraction (XRD). The consolidated iron powders, however, showed the major peaks in the X-ray diffraction pattern of the α-Fe phase, and the average crystallite size was calculated to be ca. 40 nm as determined by line broadening analysis [26]. The morphology under SEM was found to be porous coral like (Fig. 6). The consolidated iron pellet had a smooth and homogenous microstructure as confirmed by SEM. This sample had a high Rockwell C (RC) hardness of 37 as compared to the hardness of conventional iron (4–5 RC). Carbon and oxygen concentrations were 0.05 and 1.1%, respectively.

A pulsed laser pyrolysis technique has been used to study the gas phase thermal decomposition of iron pentacarbonyl, and chromium, tungsten and molybdenum

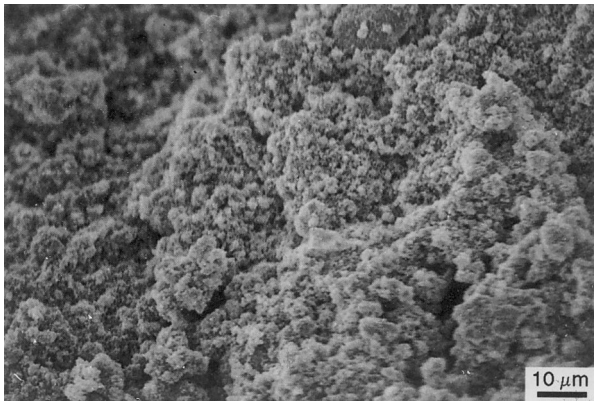

Fig. 6. SEM micrograph of the iron powder (source: [25]).

hexacarbonyl. In essence, a pulsed infrared CO_2 laser is used to heat an absorbing gas (SF_6) which then by collision, transfers its energy to the reactive substrate and bath gas (N_2). Laser pyrolysis offers dissociation energies of various transition metal carbonyls by use of the laser pyrolysis method [27].

Stabilized colloidal cobalt nanoparticles were prepared by Thomas through the thermal decomposition of $Co_2(CO)_8$ in a hydrocarbon solvent, containing a suitable polymeric material (methylmethacrylate–ethylacrylate–vinyl pyrollidone terpolymer of mole proportions 33:66:1) and about 3% methyl isobutyl ketone [28]. It should be noted that average particle size could be easily varied from ca. 20 to ca. 300 Å by variations in the reagent concentrations, temperature, and the composition of the polymeric material. Polymers with a relatively large percentage of highly polar groups promoted the growth of smaller particles. It was also found that copolymers of reasonably high molecular weight (order of 10^4 and greater) were unique in furnishing a high degree of stability to such colloids. Magnetic properties of the Co particles were measured on dried films formed by evaporation of the solvent with the polymeric material acting as a binder. In general, the magnetic properties were those to be expected from single domain particles [29]. Two unique features were observed in these nanoparticles: (1) The particles were arranged more or less in the form of a chain; and (2) they exhibited a continuous range of coercive force between limits of 200–900 Oe, while retaining constant remanence-to-saturation ratios of $0.5 \sim 0.6$ for randomly oriented samples and $0.8 \sim 0.9$ for oriented samples.

Duteil et al. have prepared Ni colloids by the reaction of $Ni(acac)_2$ (acac = acetylacetonate) and PPh_3 (Ph = phenyl) in diethyl ether with the reducing agent Et_2AlH at $-40°C$ [30]. These colloids can be isolated in the solid state and redispersed in any concentration in polar solvents such as pyridine, owing to their ligand shell mainly consisting not of PPh_3 molecules but, instead, of PPh moieties which are generated from PPh_3 during the reaction with Et_2AlH with the formation of free benzene (Eqs. (1) and (2)).

$$Et_2AlH + Ni(acac)_2 \rightarrow Et_2Al(acac) + Ni + 2H \quad (1)$$

$$PPh_3 + 2H \rightarrow C_6H_6 + PPh \quad (2)$$

HRTEM investigations of the nickel colloid, deposited on a grid from a dark brown pyridine solution, indicated a very narrow particle size distribution with an average diameter of 4 nm. The exact size of some of these particles correspond to diameters between 3.9 and 4.3 nm. Preliminary studies of the catalytic properties of the nickel colloids showed very low activities in hydrogenation reactions. For instance, the turnover frequencies for the hydrogenation of hex-2-yne to *cis*-hex-2-ene in a heterogeneous reaction was only 2 $mol_{prod}\ mol_{Ni}^{-1}\ h^{-1}$, compared with values of some hundreds using common hydrogenation catalysts of nickel or palladium. The low catalytic activity of the nickel colloids is due to the PPh ligand shell which blocks the reactants from interacting with the catalytic nickel metal.

Recently, it has been shown that CO_2 supercritical fluid dilated copolymers, such as polystyrene–block–poly(vinylpyridine) or polystyrene–block–poly(acrylic acid), selectively bind onto organometallic precursors like dimethyl-(cyclooctadiene) platinum (II) [31]. Reduction of the bound organometallic compound with hydrogen yields the corresponding metal clusters (10 nm) which remain positioned in the copolymer lattice.

3.2. Synthesis of nanostructured metal alloys from organometallics

Metal alloys are defined as solid solutions of two or more metals in varying proportions. The properties of the metal alloys are unique [32]. The general chemical synthesis methods used to prepare these metal alloys are very similar to the production of individual metals. The synthesis and microstructural study of a four-component metal alloy, commonly known as M-50 steel [33], are discussed below.

3.2.1. Two component metal alloys

Suslick et al. [24] also prepared amorphous Fe–Co alloys by irradiation of a decane solution of $Fe(CO)_5$ and $Co(CO)_3(NO)$ with a high-intensity ultrasonic probe. The composition of the Fe–Co alloys can be controlled easily by changing the ratio of relative concentrations of the precursors. The nanostructured Fe–Co alloys are porous agglomerates of small clusters of $10 \sim 20$ nm particles. The surface composition of the alloys demonstrated some small enrichment of Fe over Co. The 1:1 Fe–Co alloy showed nearly 100% selectivity for dehydrogenation of cyclohexane to yield benzene as compared to the formation of aliphatic hydrocarbons via hydrogenolysis.

Recently, metal-organic chemical vapor deposition has been applied for the preparation of supported bimetallic catalysts [34]. Nanoparticles of platinum deposited on silica were obtained by passing a gas mixture of helium, 3% hydrogen and 1 mM $Pt(Me)_2(COD)$ (COD = η^4-1,5-cyclooctadiene) over silica at 120°C. After Pt nanoparticle deposition, a gas mixture of helium, 1% hydrogen and 4 mM $Pd(\eta^3\text{-}C_3H_5)(hfacac)$ (hfacac = hexafluoroacetylacetonato ligand) was passed at

60°C to deposit a layer of Pd metal to cover Pt nanoparticles. The Pt deposition in the first step gave particles of 2.5 ~ 3.0 nm in size, while the second step resulted in bimetallic particles of 5 ~ 15 nm. The as-synthesized bimetallic nanoparticles have a unique layered structure, which is different from the regular alloy-like system, and may be quite useful as a bimetallic catalyst.

3.2.2. M50 steel

The M50 type steel (4.0% Cr, 4.5% Mo, 1.0% V, 0.8% C, 0.3% Mn with balance of Fe) produced by normal casting procedures is a martensitic steel widely used in bearing applications in the temperature range of 450 ~ 800°C [33a]. It is also one of the most popular steels used in tool manufacturing and in the aircraft industry where their applications are in main-shaft bearings in gas turbine engines. The martensitic grain sizes of this M50 steel are commonly in the order of ca. 30 μm with some dispersion precipitates in the range of a few micrometers in diameter. These relatively large carbides often act as crack initiation sites [35]. The microstructural refinement often enhances the mechanical and physical properties of the material obtained [36]. Nanostructured materials with grain sizes in the nanometric regime are expected to further provide improved mechanical properties. Therefore, nanostructural M50 specimens are expected to improve their mechanical properties, and at the same time avoid the presence of large carbides that have deleterious effects on the performance of these steels during service.

The nanostructured M50 specimens have been prepared in our laboratory in three different ways: (a) Thermochemical method [37]; (b) Sonochemical synthesis without surfactant [33e]; and (c) Sonochemical synthesis with surfactant [33e]. The prepared powders were then consolidated in a vacuum hot press (VHP).

The powders obtained by the above thermal decomposition of the metal carbonyls appeared as shiny black metallic particles. They were pyrophoric and had to be coated with degassed mineral oil for surface protection for subsequent handling. X-ray diffraction(XRD) analysis of the synthesized powders was performed, and is shown in Fig. 7a. The analysis revealed the powder to be highly disordered, since very broad peaks were obtained from 35 to 55° and from 70 to 90° in 2θ. The broad peaks are characteristic of amorphous materials as reported previously for other amorphous alloys or glassy metal powders [38]. Morphological examination of the as-synthesized powders were performed using scanning electron microscopy(SEM), transmission electron microscopy(TEM) and high resolution transmission electron microscopy(HRTEM). SEM of the powder revealed a porous structure. TEM of the powder showed that these powders are nanostructured agglomerates of about 50 nm in size (see Fig. 8). Careful examination further revealed that these agglomerates were built-up from nanostructured particles each about 4 nm. Elemental analysis was performed on the powder samples using energy dispersion analysis by X-ray(EDAX), and the composition was obtained as follows: Fe 94.2%; Cr 0.3%; Mo 0.4% and V 2.1%. As discussed earlier, a typical M50 alloy should have a composition Fe 98.7%; Cr 4%; Mo 4.5%; V 1% and C 0.8%. This compositional discrepancy was attributed to the sublimation of the $Cr(CO)_6$ and $Mo(CO)_6$ during the decomposition process. The consolidated sample also gave a

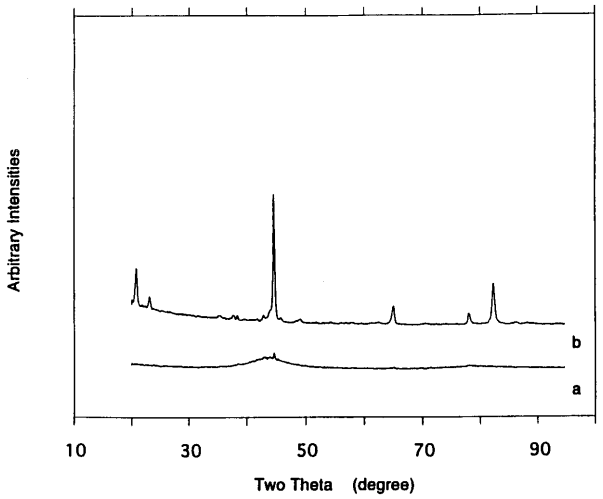

Fig. 7. X-ray diffraction analysis of M50 type steel (a) as-synthesized powders and (b) consolidated sample.

lower Cr and Mo content relative to conventional M50 steel as seen in EDAX analysis. This is illustrated in Fig. 9, where a spectrum from a large area in the specimen (30 × 30 mm) is displayed. The spectrum also shows an aluminum signal related with residues of alumina used in the polishing process. Alternative Mo and Cr precursors have been developed for the synthesis of M50 steel powders of the same stoichiometry as in the commercial product.

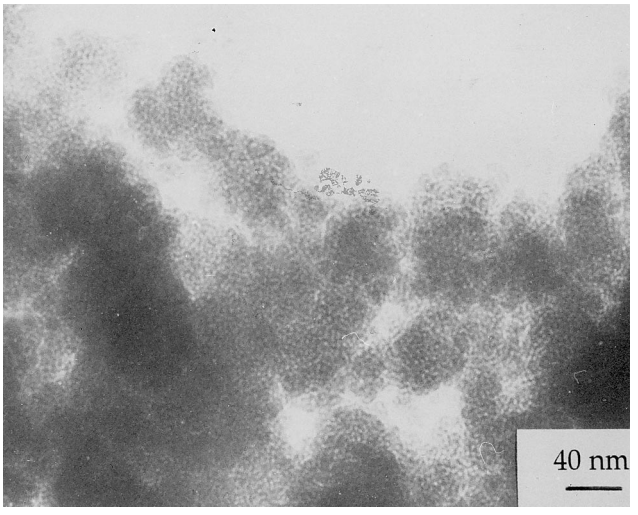

Fig. 8. Bright field TEM micrograph of the as-synthesized M50 type steel powders.

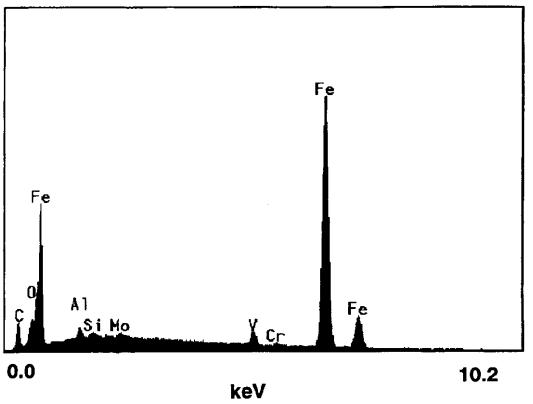

Fig. 9. An EDAX spectrum from a large area in the specimen. Fe, C, Cr, V and Mo peaks can clearly be seen.

The VHP consolidated M50 steel specimen from thermal decomposition was examined by X-ray diffraction, and shown to be crystalline nanostructured solids. In contrast to the broad X-ray diffraction peaks observed in as-synthesized powders, the diffraction peaks of these consolidated specimens were relatively sharp. The major diffraction peaks were assigned as α-Fe, and the weak peaks were from the minor carbide component (see Fig. 7b). The average size of the crystallites in the consolidated sample was about 45 nm derived from the X-ray line broadening analysis. The bright field TEM of the consolidated sample showed an average grain size of about 50 nm. A phase separation was also revealed by the microstructural contrast in the TEM [37].

The consolidated M50 steel samples were also carefully examined with HRTEM of ca. 0.17 nm resolution. Fig. 10 shows a general microstructural view of a M50 specimen obtained under bright field conditions. The image shows crystalline regions with different type of lattice fringes, which suggests different crystal orientations. The average crystallite size is about 50 nm, and the main crystalline component is α-Fe, but there are different crystalline carbides coexist with the major α-Fe phase. Small particles are precipitated in the α-Fe crystalline grains as seen in Fig. 11. This HRTEM image illustrates two different types of lattice fringes in crystalline regions. The square array of dots corresponds to an interplanar distance of ca. 0.28 nm and a $\langle 100 \rangle$ orientation in the body centered tetragonal crystal structure of these α-Fe crystallites [37]. This interplanar distance of ca. 0.28 nm is very close to the (hkl) lattice distance (0.288 nm) reported in the literature [38]. In the same image (Fig. 11), there is another set of fringes with a larger lattice spacing (area pointed by the arrows). However, these intensity variations correspond to Moire fringes, which are observed as a result of two crystalline regions stacking one to the other. Therefore, the image contrast is likely due to a crystallite precipitated into the α-Fe matrix. The diameter of this precipitated crystallite is ca. 25 nm. An insight into the nature of this crystalline precipitate can be drawn from

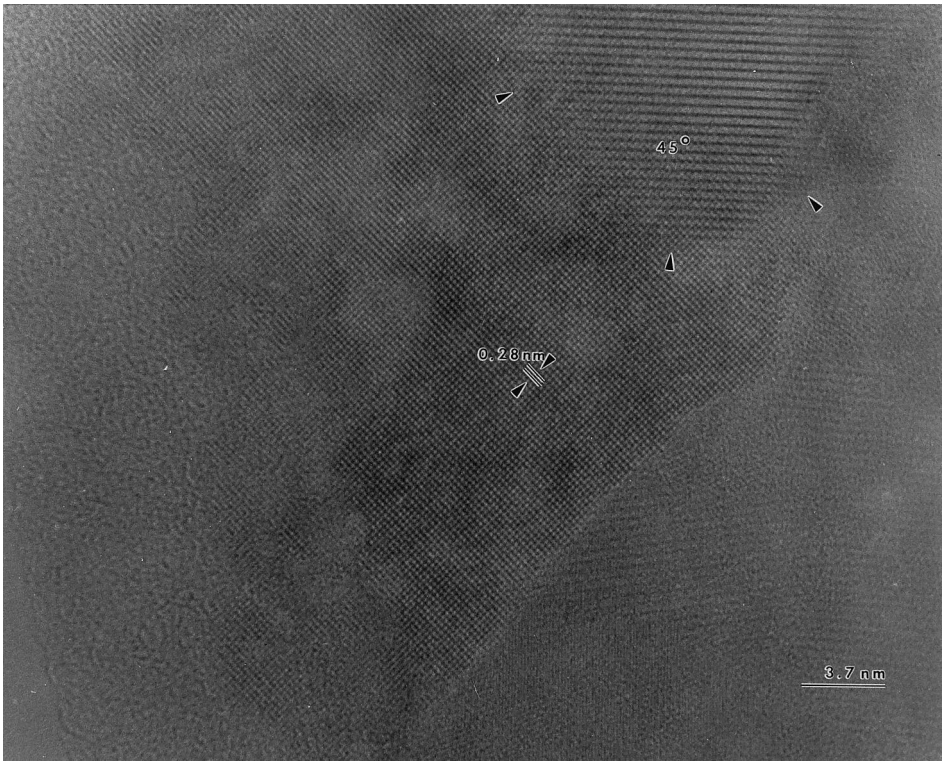

Fig. 10. HREM image of the nanostructured M50 steel. Small crystalline regions with different orientations can clearly be seen.

the relationship between the Moire and the lattice spacing in the HRTEM images. Thus, for example, in Fig. 11, the angle between the α-Fe and the Moire fringes is ca. 45°. The angle between both crystalline structures is 26°. The measured lattice spacing of the matrix and the precipitates are 0.288 and 0.508 nm, respectively. Therefore, using the theoretical expressions given by Hirch et al. [39], the lattice spacing of the crystalline precipitate is 0.217 nm. This value is close to those reported for Mo_2C [38]. Fig. 12, on the other hand, shows two different types of image contrast features. There is a set of weak lattice fringes which run almost along most of the displayed region. However, there are small islands of hexagonal arrays of dots with a dot-to-dot distance of ca. 0.30 nm (region indicated by arrows in the figure). This distance is similar to $d_{(100)} = 0.301$ nm in the hexagonal closed packed structure of molybdenum carbide (Mo_2C). The result is also illustrated from the selected area diffraction patterns obtained from this region.

One interesting aspect of this nanostructured steel is the complex diversity of the grain boundaries between those nanometric crystallites. Many different types of boundaries were found in this nanostructured material, and one example is illustrated in Fig. 13, in which an atomic resolution image of a grain boundary between

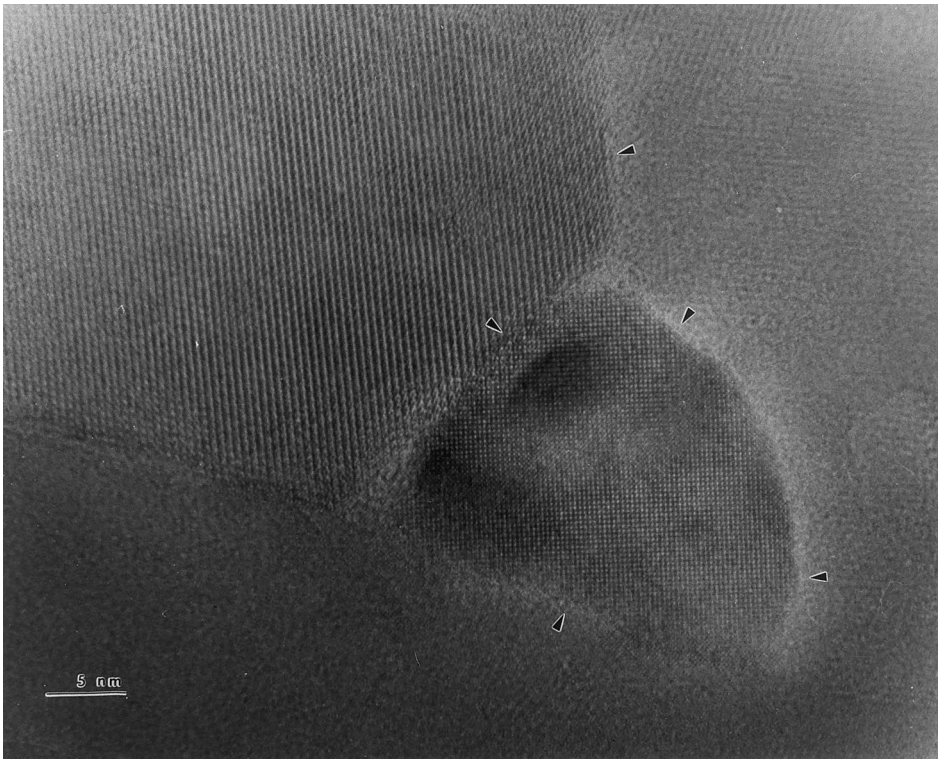

Fig. 11. HREM image showing an α-Fe grain and a small particle of ca. 25 nm in diameter precipitated in this grain.

the α-Fe grains is displayed. This image has been obtained after a numerical digitization of the original micrograph, and subsequent filtering in order to eliminate the random noise. The most important feature of this boundary is the presence of a coincidence lattice, and it can be clearly seen from the lattice planes, which are continuous across the boundary. In the nanometric crystal on the right hand side of the boundary, the angle between the lattice planes (indicated in the figure) is ca. 60°. These atomic planes are of the {100} type; therefore, the crystalline grain is oriented with a normal axis of the ⟨111⟩ type. In the nanometric crystal on the left-hand side of the boundary, the angle between the atomic planes (indicated in the figure) is ca. 54°. In this case, the planes are of the {110} and {211} types. Consequently, this nanometric grain is oriented close to a ⟨311⟩ normal axis. Part of this boundary is produced by a rotation of ca. 33° between the two crystalline grains with a rotation axis of the ⟨111⟩ type. In other terms, the boundary involves a twist mechanism from the ⟨111⟩ to the ⟨311⟩ orientations. Furthermore, this grain boundary covers a region between the two adjacent crystals in $2 \sim 3$ lattice spacing, and this suggests a tilt mechanism between the two crystallites. Therefore, the formation of this boundary is related with both twist and tilt mechanisms.

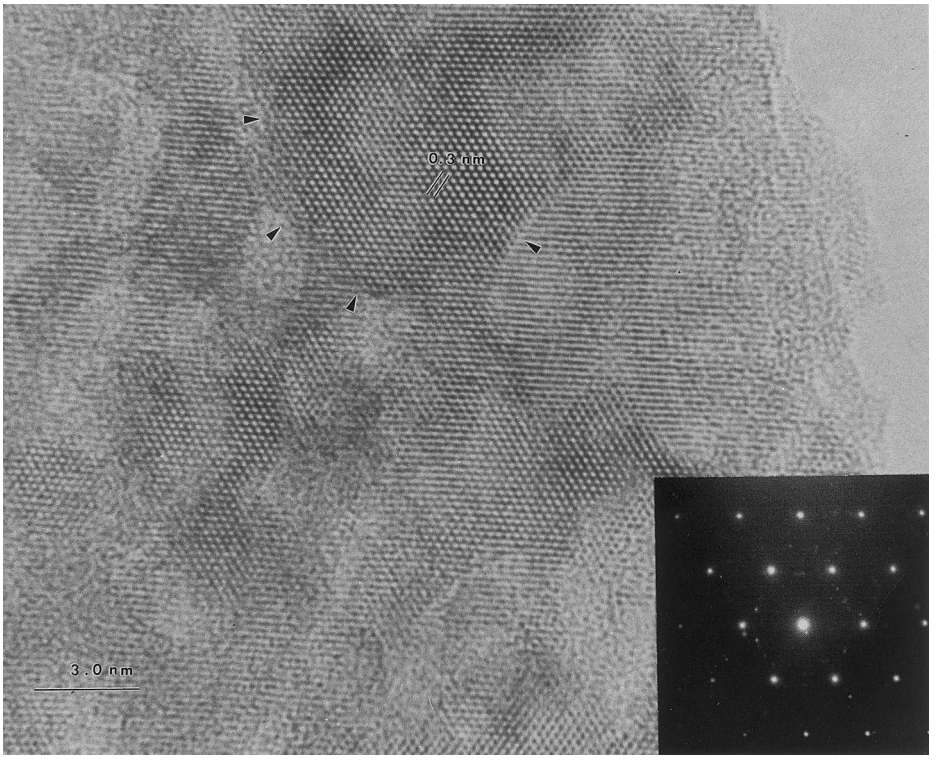

Fig. 12. HREM image which shows weak fringes associated with an α-Fe grain and also small precipitates with hexagonal array of dots. A selected area diffraction pattern from a region rich in this type of precipitates is also illustrated.

The thermally prepared M50 powders are amorphous as observed from both XRD and TEM studies. Amorphous alloys or metallic glasses are often obtained by quenching of molten alloys at an ultrahigh cooling rate in the conventional techniques [40,41]. Amorphous or glassy metal powders and thin films can be prepared via gas condensation techniques, in which hot atoms from the evaporated source are rapidly condensed onto a cold substrate [42]. In our chemical synthesis, however, the amorphous phases are formed via a decomposition of organometallic precursors in liquid decalin. The decomposition temperature was 160°C, which is far below the melting or evaporation temperatures of these metals. Thus, the mechanism in the glass formation by the carbonyl thermal decomposition ought to be quite different from either the rapid solidification or the hot metal vapor condensation process. Wonterghem et al. [19] also prepared glassy iron powders via the decomposition of $Fe(CO)_5$. According to their studies, the carbonyl decomposition was based on the growth of amorphous particles stabilized by impurity atoms present at the surface of the nanoparticles. These impurities included carbon, surfactants, and other organic solvents [14,19,43]. In our studies, chemical analysis revealed ca. 3% carbon in the as-synthesized powders. These carbon atoms could be

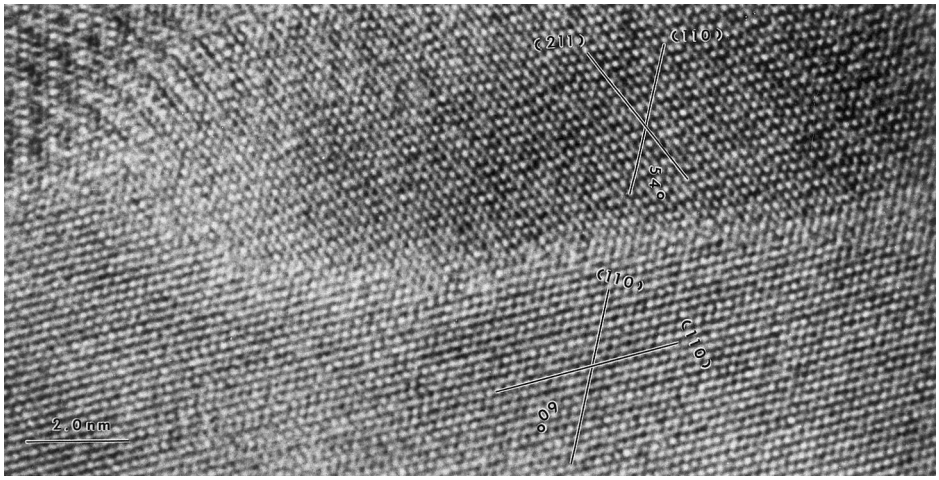

Fig. 13. Grain boundary between two different α-Fe grains. The geometrical structural properties of this boundary suggest twist and tilt mechanics in their formation.

produced as a result of chemisorption and subsequent decomposition of CO at the particle surface [19], or via the decomposition of the decalin at 160°C during the long refluxing period. Also, vanadium carbide is known to be a good grain growth inhibitor. It would be reasonable to suggest that in our synthesis the formation of amorphous powders is a combination of several factors including: (i) the presence of carbon atoms on the nanoparticle surface; (ii) the inclusion of vanadium atoms in the nanostructured powders; and (iii) the presence of decalin solvent which limited the diffusion of metal atoms surrounding the nanoparticles. Our surfactant assisted synthesis of nanostructured M50 type steels [32e] has indirectly established the above mechanism, as a narrower distribution of nonagglomerated particles of ca. 7 nm in size was obtained.

The chemical and structural characters of sonochemically prepared M50 steel powders were also studied with EDAX, SEM, and TEM. Without surfactants, the sonochemically prepared M50 powders were highly agglomerated (Fig. 14). In contrast, with surfactants the M50 steel powders prepared were much less agglomerated, and the SEM shows a porous coral-like morphology (Fig. 15) at identical magnification. The chemical analysis by EDAX in several randomly selected regions of the powder sample (with surfactant) shows the same content ratios of Fe, Cr, Mo and V as in M50 steel (Fig. 16). The TEM microstructure of the powders made without surfactants shows a very agglomerated structure composed of smaller particles having mean particle diameters of $5 \sim 10$ nm. In contrast, a more homogenous distribution of the particles is observed for powders produced with surfactants (Fig. 17), and these particles are discrete and deglomerated. The XRD analysis of the as-synthesized powders (with surfactants) revealed a rather amorphous pattern as shown in Fig. 18 with a very broad peak centered around $44 \sim 45°$ with FWHM of ca. 5° in 2θ.

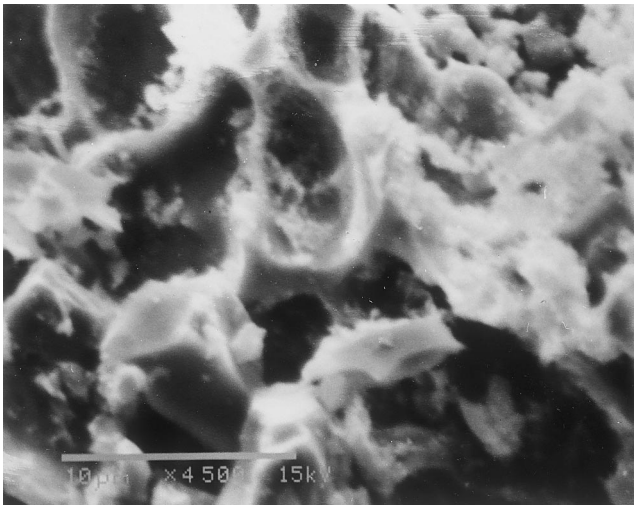

Fig. 14. SEM micrograph of sonochemically synthesized M50 steel powders (without surfactant) (source: [33e]).

The VHP compacted sonochemically prepared M50 steel specimen [32b] was analyzed with EDAX, which shows a uniform microstructure with scattered Cr-rich precipitates. The specimen is 100% dense. The carbon and oxygen content of the consolidated specimen was found to be 0.54 and 4.1%, respectively. The bright and dark field TEM micrographs of the matrix in the consolidated sample shows a distribution in grain size, and the range varies between 5 and 70 nm. TEM micrographs obtained by tilting the sample ($+5°$ to $-5°$) in the same region

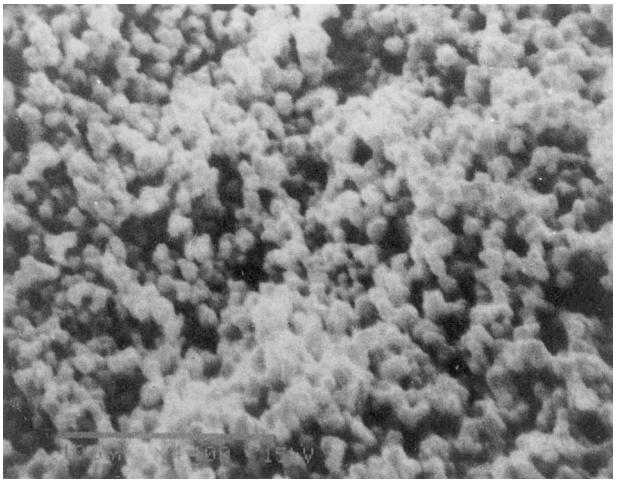

Fig. 15. SEM micrograph of sonochemically synthesized M50 steel powders (with surfactant) (source: [33e]).

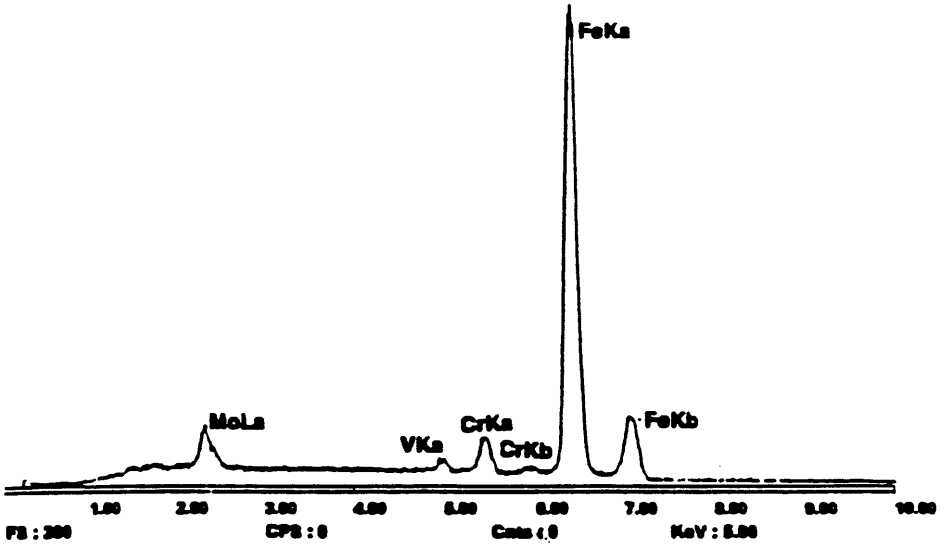

Fig. 16. EDAX analysis of sonochemically synthesized steel powders (with surfactant) (source: [33e]).

confirmed that the microstructural contrast observed is mainly due to orientation effects of α-Fe crystallites, although phase separation between the matrix and the precipitates could also contribute to this effect. The electron diffraction of the matrix showed a spotty diffraction pattern corresponding to the α-Fe bcc phase. The bright field and dark field TEM micrographs of the precipitate indicate a very

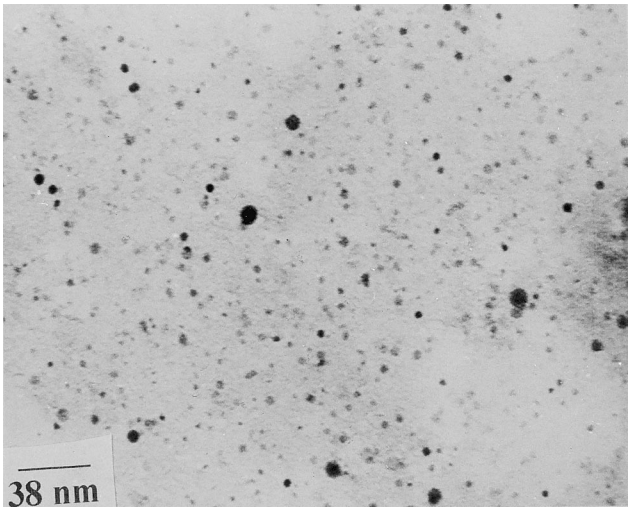

Fig. 17. TEM micrograph of sonochemically synthesized M50 steel powders (with surfactant) (source: [33e]).

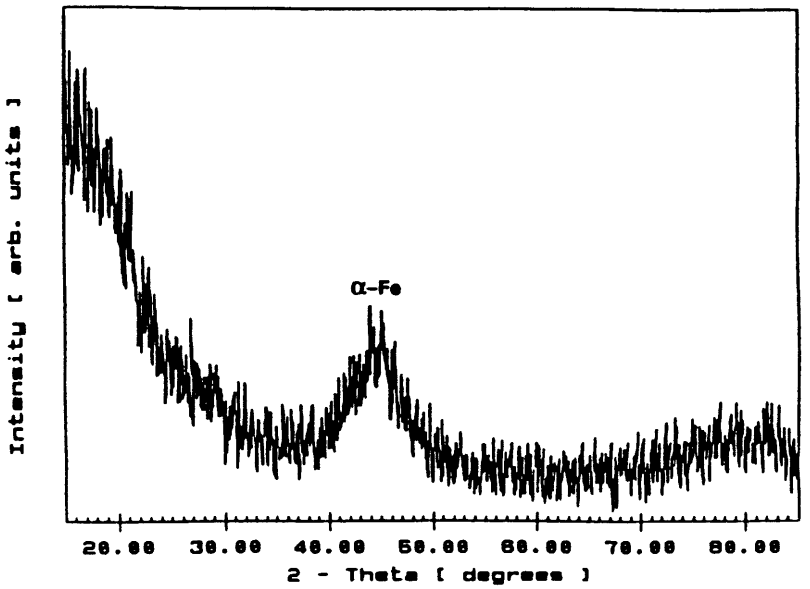

Fig. 18. X-ray diffraction pattern of the as-synthesized M50 steel powders (source: [33e]).

fine precipitate with diameters averaging ca. 10 nm. The electron diffraction pattern of the precipitate indicated that it had a CF8 structure with the best fit corresonding to the Mo_2C phase.

In short, the microstructure of the thermally prepared M50 specimen is based in the α-Fe matrix with crystalline grain of 50 nm in diameter. There are also nanoparticles of a few nanometers precipitated in the matrix and in the grain boundaries. HRTEM elucidate the crystalline precipitates to be Mo_2C phase. The nanostructured M50 steel specimen displays complex grain boundaries between nanometric crystallites. HRTEM low angle boundary studies suggest both twist and tilt mechanisms in these boundary formation. The nanostructured M50 steel powders made by both thermal and sonochemical decomposition are amorphous as identified by XRD and TEM, and it is believed to be a collected effect of foreign atoms and solvent molecules on the nanoparticle surface. The thermal decomposition of metal carbonyls produced nanostructured metal powders of lower Cr and Mo content relative to commercial M50 steel. The newly developed Cr and Mo precursors gave rise to nearly stoichiometric M50 steel powder in the sonochemical decomposition. The examination of M50 steel powders synthesized with and without polymeric surfactants demonstrated that surfactants are very effective in producing fairly homogenous and discrete multi-component alloy powders. The mean particle size of 7 nm was obtained for the ultrasound assisted synthesis of these metal nanopowders. EDAX analysis proved that the powders synthesized in the presence of a surfactant exhibited high compositional homogeneity on the nanometer scale.

4. Conclusion

We have outlined several techniques for the synthesis of nanostructured metals and metal alloys. Considerable opportunities now exist for synthesizing nanophase materials with a variety of new architectures at nanometer length scales. The real future of nanostructured metals and metal alloys and other nanostructures as well, will depend on our ability to change significantly for the better, the properties of materials by structuring them artificially on nanometer scales, and on developing economic and environmentally responsible methods for producing these materials in commercially viable quantities. Synthesis of nanoparticles from organometallics is a rapidly growing research area with a great potential to make technologically advanced and useful materials. The realization of this potential will require multidisciplinary interactions and collaborations between chemists, materials scientists, and engineers, in order to control and improve the properties of nanophase materials.

Acknowledgements

KEG acknowledges partial support from ONR and a NSF-Conacyt (Mexico) Cooperative grant. We also acknowledge Dr S.P Rangarajan for the synthesis of the powders, Professor A. Garcia-Ruiz of IPN Mexico for the XRD analysis and refinement studies; Dr Gan-Moog Chow of the Naval Research Lab. for some of the additional TEM data; and Dr Chi Law of Pratt and Whitney, UTC East Hartford, CT for consolidation of the samples.

References

[1] (a) H. Gleiter, Adv. Mater. 4 (1992) 474. (b) R. Birringer, H. Gleiter, in: R.W. Cahn (Ed.), Encyclopedia of Materials Science and Engineering, suppl. vol 1, Pergamon, Oxford, UK, 1988, p. 339.
[2] R.W. Seigel, Nanostruct. Mater. 3 (1993) 1.
[3] R.W. Seigel, Mater. Sci. Eng. B19 (1993) 37.
[4] (a) R.W. Cahn, Nature 348 (1990) 389. (b) R. Dagani, Chem. Eng. News 72(47) (1992) 18. (c) Gleiter, H. Nanostruct. Mater. 6 (1995) 3. (d) D. Chakravorty, A.K. Giri, in: C.N.R. Rao (Ed.), Chemistry for the 21st Century: Chemistry of Advanced Materials, 217, Blackwell Scientific, London, 1993.
[5] (a) Y. Yoshizawa, S. Oguma, Y. Yamaguchi, J. Appl. Phys. 64 (1988) 6044. (b) H.J. de Witt, C.H.M. Wittmer, F.W.A. Dirne, Adv. Mater. 3 (1991) 356.
[6] (a) D.D. Beck, R.W. Seigel, J. Mater. Res. 7 (1992) 2840. (b) E. Boakye, J. Colloid. Interface Sci. 163 (1994) 120.
[7] (a) C.R. Aita, Nanostructr. Mater. 4(3) (1994) 257. (b) K.J. Balkus Jr., in: K.E. Gonsalves, G.M. Chow, T.D. Xiao, R.C. Cammarata (Eds.), Molecularly Designed Ultrafine/Nanostructured Materials, Materials Research Symposium Proceedings, vol. 351, 1994, p. 437. (c) T. Kameyama, J. Mater. Sci. 25 (1994) 1058.
[8] (a) J. Rivas, J. Magn. Magn. Mater. 122 (1993) 1. (b) K.E. Gonsalves, T.D. Xiao, in: B.I. Lee, E.J.A. Pope (Eds.), Chemical Processing of Ceramics, Dekker, New York, 1994, p. 359. (c) W.

Chang, Nanostruct. Mater., 4(3) (1994) 345. (d) J. Phalippou, in: B.I. Lee, E.J.A. Pope (Eds.), Chemical Processing of Ceramics, Dekker, New York, 1994, p. 265. (e) C.J. Brinker, J. Schener, Sol–Gel Science, The Physics and Chemistry of Sol–Gel Processing, Academic, Boston, 1990.
[9] R.W. Seigel, in: R. Cahn (Ed.), Materials Science and Technology, vol. 15, VCH, Weinheim, 1991, p. 583.
[10] (a) S.K. Ganapathi, D.A. Rigney, Scripta. Metall. Mater. 24 (1990) 1675. (b) H.J. Fecht, E. Hellstern, Z. Fu, W.L. Johnson, Adv. Powder Metall. 1–2 (1989) 111. (c) E. Hellstern, H.J. Fecht, Z. Fu, W.L. Johnson, J. Appl. Phys. 65 (1989) 305. (d) C.C. Kock, J.S.C. Jang, S.S. Gross, J. Mater. Res. 4 (1989) 557.
[11] P.A. Psaras, H.D. Langford (Eds.), Advancing Materials Research, US National Academy of Engineering and National Academy of Sciences, National Academy Press, Washington, DC, 1987, p. 203.
[12] (a) V.K. LaMer, R.H. Dinegar, J. Am. Chem. Soc. 72 (1950) 4847. (b) J.T.G. Overbeek, Adv. Colloid. Interface Sci. 15 (1982) 251.
[13] (a) W. Chang. Nanostructr. Mater. 4(3) (1994) 345. (b) H. Hahn, R.S. Averback, J. Appl. Phys. 67 (1990) 1113.
[14] T.W. Smith, D. Wychick, J. Phys. Chem. 84 (1980) 1629.
[15] (a) W. Hieber, R. Werner, Chem. Ber. 90 (1957) 286. (b) W. Hieber, N. Kahlen, Chem. Ber. 91 (1958) 2234.
[16] (a) J. Dewar, H.O. Jones, Proc. R. Soc. London, Ser. A 76 (1905) 564. (b) H.G. Cutforth, P.W. Selwood, J. Am. Chem. Soc. 65 (1905) 2414.
[17] (a) T.H. Whitesides, J.P. Neilan, J. Am. Chem. Soc. 95 (1973) 5811. (b) H.W. Whitlock Jr., Y.N. Chuah, J. Am. Chem. Soc. 87 (1965) 3605.
[18] I. Nakatani, M. Hijikata, K. Ozawa, J. Magnet. Magnet. Mater. 122 (1993) 10.
[19] J. Wonterghem, S. Morup, S.W. Charles, S. Wells, J. Villadsen, Phys. Rev. Lett. 55 (1985) 410.
[20] S.W. Charles, J. Popplewell, in: E.P. Wohlfarth (Ed.), Ferromagnetic Materials, vol. 2, North-Holland, Amsterdam, 1980, p. 509.
[21] (a) B.S. Clausen, S. Morup, H. Topsoe, Surf. Sci. 106 (1981) 438. (b) S. Morup, H. Topsoe, B.S. Clausen, Phys. Scr. 25 (1982) 713.
[22] (a) G. Le Caer, J.M. Dubois, M. Pijolat, V. Perrichon, P. Bussiere, J. Phys. Chem. 86 (1982) 4799. (b) C.B. Ma, T. Ando, D.L. Williamson, G. Krauss, Metall. Trans. A 14 (1983) 1033.
[23] X. Cao, Y. Koltypin, G. Kataby, R. Prozorov, A. Gedanken, J. Mater. Res. 10 (1995) 2952.
[24] K.S. Suslick, T. Hayeon, M. Fang, Chem. Mater. 8 (1996) 2172.
[25] K.E. Gonsalves, S.P. Rangarajan, A. Garcia-Ruiz, C.C. Law, J. Mater. Sci. Lett. 15 (1996) 1261.
[26] J. Schneider, Acta. Crystallogr. A43 (1987) 295.
[27] (a) D.M. McMillen, K.E. Lewis, G.P. Smith, D.M. Golden, J. Phys. Chem. 8 (1982) 709. (b) W.M. Shaub, S.H. Bauer, J. Chem. Kinet. 7 (1975) 509.
[28] J.R. Thomas, Chem. Commun. (1965) 2914.
[29] F.E. Luborsky, T.O. Paine, J. Appl. Phys. 31 (1960) 68S.
[30] A. Duteil, G. Schmid, W. Meyer-Zaika, J. Chem Soc. Chem Commun. (1995) 31.
[31] (a) J.J. Watkins, in: K.E. Gonsalves; L. Merhari, et al. (Eds.), MRS Proc., vol. 584 (in press) (2000). (b) J.J. Watkins, J.J. McCarthy, Polym. Mater. Sci. Eng. 73 (1995) 158.
[32] (a) M.J. Tracy, J.R. Groza, Nanostructure Mater. 1 (1992) 369. (b) K. Higashi, T. Mukai, S. Tanimura, A. Inoue, K. Masumoto, K. Kita, K. Ohtera, J. Nagahora, Nanostruct. Mater. 26 (1992) 191.
[33] (a) K.E. Gonsalves, T.D. Xiao, G.M. Chow, C.C. Law, Nanostructure Mater. 4 (1994) 139. (b) K.E. Gonsalves, S.P. Rangarajan, C.C. Law, C.R. Feng, G.-M. Chow, A. Garcia-Ruiz, ACS Symp. Series 622 (1996) 220. (c) C.R. Feng, G.M. Chow, S.P. Rangarajan, X. Chen, K.E. Gonsalves, C.C. Law, Nanostruct. Mater. 8 (1997) 45. (d) K.E. Gonsalves, S.P. Rangarajan, in: E. Ma, B. Fultz, R. Shull, J. Morral, P. Nash, (Eds.), Chemistry and Physics of Nanostructures and Related Non-Equilibrium Materials, TMS, 1997, p. 149. (e) K.E. Gonsalves, S.P. Rangarajan, J. Appl. Polym. Sci. 64 (1997) 2667. (f) K.E. Gonsalves, US patents (1987) 4,842,641; (1996) 5,589,011; (1999) 5,984,996.
[34] J.-C. Hierso, R. Feurer, J. Poujardien, Y. Kihn, P. Kalck, J. Mol. Catal. 135 (1998) 321.

[35] (a) F. Kayser, M. Cohen, Metal Prog. 61 (1952) 79. (b) W.B. Pearson, A Handbook of Lattice Spacing and Structure of Metals and Alloys, vol. 1, Pergamon Press, New York, 1958. (c) K. Kuo, J. Iron Steel Inst. 173 (1953) 363.
[36] (a) H. Gleiter, Nanostructure Mater. 1 (1992) 1. (b) K.E. Gonsalves, X. Chen, Inorganic nanostructured materials, and refs therein, in: J.C. Salamone (Ed.), Polymeric Materials Encyclopaedia, vol. 5, CRC Press, Boca Raton, FL, 1996, p. 3256. (c) K.E. Gonsalves, S.P. Rangarajan, J. Wang, Chemical synthesis of nanostructured metals, metal alloys and semiconductors, in: H. Nalwa (Ed.), Handbook of Nanostructured Materials and Nanotechnology, vol. 1, Academic Press, 1999, p. 1.
[37] K.E. Gonsalves, T.D. Xiao, G.M. Chow, C.C. Law, Nanostruct. Mater. 4 (1994) 132.
[38] Selected Powder Diffraction for Metals and Alloys, Int. Center for Diffraction Data, JCPDS, Swarthmore, PA, vol. I and II, 1978.
[39] P. Hirch, Electron Microscopy of Thin Crystals, Krieger, Huntington, New York, 1977.
[40] A. Inoue, J. Saida, T. Masumoto, Metall. Trans. 19A (1988) 2315.
[41] F.E. Laborsky, in: E.P. Wohlfarth (Ed.), Ferromagnetic Materials, vol. 1, North–Holland, Amsterdam, 1980, p. 451.
[42] M.G. Scott, R. Maddin, in: N.J. Grant, B.C. Giessen (Eds.), Rapidly Quenched Metals, MIT Press, Cambridge, MA, 1976, p. 240.
[43] E. Paoirer, P. Horny, H. Balard, B. Anthone, C. Petipab, A. Martinet, J. Colloid Interface Sci. 94 (1983) 220.